ANNEX A2

CO_2 Storage Liabilities in the North Sea –

An Assessment of Risks and Financial Consequences

Cap Rock
Study

Simon Mathias
Durham University

Status	**FINAL Draft**
Date	**16th May 2012**
Issued by	**Stephen Jewell**

Annex A2 - Contents

1.0 Introduction - Leakage through caprocks

Storage of CO_2 in geological reservoirs relies on the existence of an extensive and robust cap-rock. Whether in a gas form or a dense phase liquid, CO_2 will most often be less dense than the formation water typically expected to reside in the range of saline aquifers and depleted oil and gas reservoirs currently under consideration. Consequently, mobile free-phase CO_2 is expected to be buoyant and may ultimately migrate back up to the seabed or atmosphere unless a suitable barrier is in place.

Note that it is necessary to distinguish between mobile free-phase CO_2, residually trapped CO_2 and dissolved aqueous phase CO_2. The latter is generally expected to be denser than the host formation fluid and therefore negatively buoyant. Residually trapped CO_2 is CO_2 trapped by formation water in the pore-space due to interfacial tension between the CO_2 and formation water. It is only the free-phase CO_2 which is mobile and positively buoyant. The fraction of mobile and positively buoyant CO_2 in the reservoir is widely expected to decrease with time (MacMin et al., 2011). Nevertheless, a large proportion of the CO_2 is generally expected to remain mobile and positively buoyant for 1000s of years.

The International Energy Agency (IEA) have recently published a very comprehensive report concerning caprock systems for CO_2 geological storage (IEAGHG, 2011). The report looks at a range of issues including seal potential, geomechanics, hydrodynamics, geochemical interactions and risk assessment. The term seal potential is often used to discuss the capillary sealing that comes about due to interfacial tension between two fluids. Geomechanics is discussed in the context of caprock integrity. As CO_2 is injected into a reservoir, pore pressure can be expected to increase, and as a consequence, mechanical failure of the cap-rock can occur. “Hydrodynamics”, in this context, refers to the effect of overpressure in the reservoir on capillary sealing.

Interestingly, in their risk-assessment discussion (of IEAGHG, 2011), discussed leakage rates are all in terms of leakage through faults and fractures within the caprock as opposed to the caprock itself. Such issues are discussed in separately in our report in the section on leakage through faults. The text in our contribution on leakage through caprocks below is more focused on explaining the physical basis behind why the risk of direct leakage of CO_2 through intact caprocks (excluding fractures and faults) is unlikely to be significant.

This section starts with a brief introduction to the relevant caprock systems present in the UK North Sea. The report discusses relevant hypotheses and experimental data concerning capillary sealing in the context of CO_2 brine mixtures, followed by the technical basis for assessing caprock integrity in the context of CO_2 injection induced mechanical failure. Finally the section summarises and concludes, leading into the section on leakage through faults.

The text within this section builds heavily on the report of IEAGHG (2011) although emphasis has been changed towards intact caprock and caprock systems of the North Sea. Our text also reveals insights from several additional studies leading to improved understanding concerning interfacial tension of CO_2-brine mixtures, stress dependent permeability of anhydrites and pore-pressure-fracture-pressure coupling.

2.0 Reservoirs and caprocks

The UK North Sea is divisible into two major geological provinces; the Southern North Sea Basin (SNSB) and the combined Central, Moray Firth and Viking graben with associated shelfal areas herafter referred to as the Northern North Sea Basins (NNSB). The potential CO_2 storage sites and associated seals differ between the two basins and will be discussed separately.
All of SNSB gas has been produced from the the Carboniferous, the Lower Permian Rotliegend Group, and the Triassic Bacton Group (including the Bunter Sandstone and Hewitt Sandstone Member) reservoir formations (Duguid and Underhill, 2010). The main source rock consists of coal belonging to the Upper Carboniferous. Trapped gas within the Carboniferous is due to a combination of intra-Carboniferous seals and the Basal Permian (Rotliegend Group) Silverpit Claystone seal which occurs in the northern part of the SNSB. In the southern part of the SNSB, Carboniferous sandstones typically subcrop the Leman Sandstone (Rotliegend Group) and no seal exists.. Trapped gas in the Rotliegend Sandstones has generally been confined by thick layers of evaporites associated with the Zechstein Group formation. Trapped gas in the Bunter Sandstones has largely been confined by overlying halites in the Triassic Haisborough Group (HG) (see Fig. 1a). Many of these caprock formations are 100s to 1000s m thick (e.g. Fig. 1b).

The NNSB contains oil, condensate and gas trapped in a large variety of reservoirs ranging in age from Devonian to Eocene and including sandstone, limestone, chalk and rarely fractured basement rocks (Gluyas & Hichens, 2003). The principle seals are however fewer. The main ones are the Upper Jurassic Heather and overlying Kimmeridge Clay formations; Palaeocene and Eocene mudstones; and intra-Cretaceous seals in the Moray Firth area. Locally, seals also exist within the Devonian, Carboniferous, Pernian, Triassic, Middle Jurassic, Upper Cretaceous Chalk and Tertiary while diapiric salt can also act as a side seal in parts of the Central Graben.

There is considerable experience concerning the observation of gas being trapped for geological timescales underneath low permeability caprocks such as shales and evaporates in the SNSB. Furthermore, discoveries such as 'Fizzy' (block 50/26b) and Oak (block 54/1b) in the Rotliegend Group represent natural examples for long term storage of CO_2 (Yielding et al., 2011). It has also been demonstrated that the Miller Field in the NNSB was for about 50 million years a natural CO_2 storage site before oil entered the trap (Haszeldine et al, 2006) and indeed the petroleum remains rich in CO_2.

At the well-known Sleipner operation in the Norwegian North Sea, CO_2 has been injected at a rate of around 1 Mt/year into the Utsira Sand, a major saline aquifer of the late Cenozoic age, since 1996 (Chadwick et al., 2010). Time-lapse seismic monitoring data has allowed the visualisation of CO_2 trapped underneath an overlying 200 to 300 m shale cap rock. Fig. 2 shows the underlying topography of the cap rock (the colors) and the delineated extent of the CO_2 plume (the grey, obtained from time-lapse seismic). The buoyant drive of the CO_2 plume has allowed the CO_2 to migrate into the topographical highs underneath the caprock.

2.1 Permeability of intact caprocks

Most anticipated caprocks in the Southern North Sea are comprised of either shales or evaporites (anhydrites or halites). Fig. 3a compares pemeabilities (see Chapter on faults for a detailed definition of permeability) of shales and sandstones for a number of different reservoir units from Germany and Norway. Fluid flow in porous media is generally controlled by Darcy's law, which

stipulates that flow per unit area, q [m / s], is found from $q = - k J / \mu$ where k [m^2] is permeability, (Bear, 1972) J [Pa / m] is pressure gradient and μ [Pa s] is fluid viscosity. Typically, permeability is measured in milli-Darcies (mD) where 1 mD = 10^{-15} m^2. A good reservoir rock typically has a permeability of 50 to 1000 mD for geological storage of CO_2. A good seal might be expected to have a permeability < 10^{-4} mD. Certainly, many shales can be expected to have sufficiently low permeability but there are also many exceptions. Normally there is a relatively strong correlation between permeability and porosity for sandstones. In contrast, shales exhibit very little correlation. This is rather demonstrative of the fact that the description of shale tends to cover a multitude of different rock types including clays, mudstones and low permeability sandstones. Horsrud et al. (1998) define shale as any rock containing "a certain amount of clay minerals (using a limit of about 30% clays), thus providing a continuous matrix of clay".

Few measurements of permeability of evaporites have been made due to its inherently low permeabilities. Nevertheless, a review of measurement presented in the literature (in particular, Beauheim and Roberts, 2002), Evans and Holloway (2009) suggests that permeabilities of halite typically range from 10^{-9} to 10^{-6} mD and anhydrite permeability is around 10^{-5} mD. Bennion and Bachu (2007) measured the permeability of an Alberta Basin (Canada) anhydrite to be 3.54×10^{-4} mD. De Paola et al. (2009) observed intact anhydrite from the Umbria-Marche Apennines to be effective stress fabric orientation dependent (see Fig. 3b) and ranging between 10^{-6} and 10^{-4} mD. Hangx et al. (2010a) found permeability of intact Zechstein anhydrite to insufficient to measure using argon gas permeametry indicating that the permeability of their samples should be < 10^{-6} mD. It can be appreciated that intact evaporites are generally expected to be particularly effective low permeability seals. The subject of deformed evaporates is discussed subsequently in the section on caprock integrity.

Low permeability implies low rates of leakage. However, more importantly for gas trapping, low permeability implies that the rock matrix is comprised of very small pore-throat sizes. As to be explained, the interfacial tension that develops between gas and liquids within these small pore-throats can lead to zero flow in many instances.

3.0 Capillary sealing

3.1 Air entry pressure and capillary pressure

For a liquid-gas or liquid-liquid interface the liquids behave as if covered by an elastic membrane in a constant state of tension (Fig. 4). Molecules of liquids tend to experience greater attraction to similar molecules than to molecules of other fluids. As a consequence, the net attraction of similar molecules tends to cause a liquid-gas or liquid-liquid interface to contract as if in a state of tension. The nature of this contraction is described by two physical properties, the interfacial tension (IFT), γ [Pa/m], and the contact angle, Θ [deg].

The value of IFT is specific to the two fluid combination being considered. The contact angle is dependent on the properties of the two fluid combination of concern in conjunction with the rock surface within a given pore-structure. Fig. 5 shows a schematic of blobs of two different fluids situated on the surface of a given rock. Fig. 5a shows a wetting fluid, whereby the fluid is attracted to the rock surface and spreads. Fig. 5b shows a non-wetting fluid, whereby the fluid contracts within itself. Small contact angles imply high wettability and large contact angles (> 90^o) imply a non-wetting fluid.

Now consider a capillary tube of diameter, D [m], situated within a bath of water, as in Fig. 6. In this case air is the other fluid. Because the tube is water wet, water is attracted to the sides of the tube. This gives rise to a meniscus. The contact angle between the water and the tube is as indicated. The IFT between the water and air leads to water being sucked up the tube. A simple force balance reveals that the distance to which the fluid is sucked up, H [m], can be found from

$$H = 4 \gamma \cos \Theta / (D \rho_w g) \quad (1)$$

where ρ_w [kg/m^3] is the water density and g [m/s^2] gravitational acceleration.

The column of water, H, can be understood as a pressure = $\rho_w g H$. For air to displace this column of water in the tube, the air pressure would need to exceed the pressure of the water by a value of $\rho_w g H$. Hence, in some disciplines, e.g. hydrology, $\rho_w g H$ is referred to as the air-entry pressure, P_e [Pa]. Rather, the air-entry pressure of this capillary tube can be calculated from

$$P_e = \rho_w g H = 4 \gamma \cos \Theta / D \quad (2)$$

Now let us consider the so-called capillary pressure, $P_c = P_g - P_w$, where P_g and P_w are the water and gas pressures, respectively, within the representative elementary volume (REV) of concern. To empty the capillary tube of water, P_c must be greater than P_e.

3.2 Capillary bundle model

When dealing with multi-phase fluid mixtures in porous media it is common to envisage the pore-structure as containing a bundle of capillary tubes of varying pore-size diameters. In this way, a pore-structure is described by a pore-size distribution.

Consider the pore-size distribution for a sandstone rock shown in Fig. 7. The plot tells us that 60% of the pore-volume contains pores of a diameter less than 288 μm. The air-entry pressure (for a water-air system) of a 288 μm pore is 1000 Pa. Therefore, 60% of the pore-volume has an air-entry pressure > 1000 Pa. It follows that if the capillary pressure (recall $P_c = P_g - P_w$) is 1000 Pa, 60% of the pore-space continue not to allow air in, and therefore remain saturated with water.

Note that at 500 Pa, the sample is fully saturated with water. This is because almost all the pores are of a diameter less than 576 μm. Therefore even though the air-pressure is greater than the water pressure (as indicated by the positive capillary pressure), all the pores resist the air because all the pores have air-entry pressures greater than 500 Pa. In this case, it can be said that the minimum air-entry pressure of the pore-size distribution associated with this rock is 500 Pa. This pressure is often referred to as the capillary-threshold-pressure, P_{cT} [Pa].

3.3 Static gas columns

Now consider an oil (analogous to a CO_2) plume within a reservoir rock accumulated underneath a cap rock formation as in Fig. 8. The rock is water wetting. Because the cap rock pores are significantly smaller than those of the reservoir rock, the oil is unable to enter (and displace currently residing water within) the caprock unless the capillary pressure exceeds the capillary-threshold-pressure of the cap rock. Note that water (the wetting fluid) is capable of freely entering should a connected water-pathway through the gas be developed (Teiger et al., 2005).

If the height of the underlying gas column is H [m], the buoyancy pressure (force unit area) associated with the column will be $(\rho_w - \rho_g)\, g\, H$ [Pa], where ρ_g is the gas density (providing $\rho_w > \rho_g$). By consideration of the minimum air-entry pressure of the caprock, it follows that the maximum gas column that can be sustained beneath the caprock is found from

$$H_{max} = P_{cT} / (\rho_w - \rho_g)\, g = 4\, \gamma \cos \Theta / (\rho_w - \rho_g)\, g\, D_{max} \quad (3)$$

where D_{max} [m] is the size of the largest pore-throat-size with a significant presence within the caprock formation.

3.4 Estimation of capillary threshold pressure by mercury intrusion

Estimation of capillary threshold pressure for a given rock is often obtained using a mercury porosimeter. Such an apparatus typically involves monitoring the cumulative volume of mercury injected into a dried (i.e., air filled) cylindrical plug of rock (typically 1 cm diameter and 4 to 5 cm in length) as injection pressure is gradually increased.

The resulting data for a given rock sample typically takes the form of the plot in Fig. 9. It is often common to use Eq. 2 to convert such data to an estimate of pore-size distribution (as in Fig. 7) (e.g. Daniel and Kaldi, 2008). However, such a step is arguably unnecessary because the main term of interest is the so-called capillary-threshold-pressure, P_{cT} [Pa]. Schlomer and Krooss (1997) identify three pressures of interest (see Fig. 9): (1) The pressure at which mercury starts to penetrate into the largest pores, denoted as entry pressure (RP); (2) the pressure at which there is an inflection point (PP), as this denotes the mode of an inferred pore-size distribution; (3) the intersection of the tangent to PP with the pressure axis (DP). Schlomer and Krooss (1997) call this later term a displacement pressure (DP) and present measurements of DP and permeability for a number of different shales from lithologies associated with the North Sea (see Fig. 10). Here, DP can be seen to range from 1 to 200 MPa.

Earlier it was suggested that low permeability rocks imply high capillary pressures. This idea comes about by combining the capillary tube model (Eq. 2) with Poiseuille's formula for steady laminar flow through a cylindrical pipe, giving rise to the so-called Leverett (1940) scaling rule:

$$k / \phi \propto (\gamma \cos \Theta / P_{cT})^2 \quad (4)$$

where k [m^2] is permeability and ϕ [-] is porosity. Consequently many different empirical correlations have been proposed that relate permeability to capillary threshold pressure (e.g. Swanson, 1981 and Huet et al., 2005 and references therein). However, the results in Fig. 10 shows that significant caution should be given in this respect.

Nevertheless, the results in Fig. 10 can be used to infer a range of sealing efficiency that should be expected from North Sea caprocks in the context of CO_2 storage. But first, these results must be transformed from those relevant to mercury and air systems to those for CO_2 and brine systems. Consideration of Eq. 2 suggests that this can be achieved using

$$P_{cT,\text{Brine-CO2}} = P_{cT,\text{Air-Hg}}\, (\gamma_{\text{Brine-CO2}} \cos \Theta_{\text{Brine-CO2}}) / (\gamma_{\text{Air-Hg}} \cos \Theta_{\text{Air-Hg}}) \quad (5)$$

where $P_{cT,\text{Brine-CO2}}$, $\gamma_{\text{Brine-CO2}}$, $\Theta_{\text{Brine-CO2}}$, $P_{cT,\text{Air-Hg}}$, $\gamma_{\text{Air-Hg}}$, $\Theta_{\text{Air-Hg}}$ are the capillary threshold pressure, interfacial tension and contact angle for CO_2 and brine mixtures and Hg and air mixtures,

respectively. Schlomer and Krooss (1997) report that for the conditions used to obtain Fig. 10, $\gamma_{Air\text{-}Hg}$ = 0.471 N/m and $\Theta_{Air\text{-}Hg} = 140^o$.

Much work has gone into obtaining data concerning $\gamma_{Brine\text{-}CO2}$ at different pressures, temperatures and salinities. More recently, Chalbaud et al. (2009) have found that the pressure temperature dependence drops out if one instead considers the density difference between the CO_2 and brine. In this respect, Fig. 11 summarises a wealth of data for different pressures and temperatures, from which it can be seen that $\gamma_{Brine\text{-}CO2}$ = 0.0025 to 0.005 N/m. Chalbaud et al. (2009) also provide a simple correlation model (shown as modelled in Fig. 11).

Similar efforts have gone into measuring $\Theta_{Brine\text{-}CO2}$ for micas and quartz (see Figs. 12 and 13, after Chiquet et al., 2007). For mica, $\Theta_{Brine\text{-}CO2}$ goes up with increasing CO_2 pressure and salinity, ranging from 15^o to around 70^o. For quartz, $\Theta_{Brine\text{-}CO2}$ ranges from 15^o to around 35^o. Chiquet et al. (2007) argue that the rise in brine contact angle with increasing CO_2 pressure implies that wettability of CO_2 in the rock increases in the presence of CO_2. Further supporting this argument, Wollenweber et al. (2010) found that CO_2 capillary breakthrough pressure, measured by gas breakthrough testing of a Cretaceous marlstone caprock from the Munsterland Basin, decreased following repeated contact with CO_2 (see Fig. 14).

A significant problem with using mercury displacement data in this respect is that core-scale properties are unlikely to apply at caprock scale due to heterogeneities (in both vertical and horizontal directions) in the caprock formations of concern. Naylor et al. (2011) argue that a better source of information can be found from observed pre-production column heights of natural gas in analogous reservoir formations of interest. Naylor et al. (2011) go on to provide a quantitative framework to convert known gas column heights to maximum CO_2 column heights. Although pre-production column height data is not provided, the article presents data concerning the appropriate conversion factors for various Southern North Sea reservoirs. Naylor et al. (2011) calculate that sustainable CO_2 column heights in Southern North Sea reservoirs are likely to be a factor of 0.7 to 1.3 of the size of gas column heights previously observed.

3.5 Effect of overpressure on capillary sealing

Earlier in Eq. (3) it was suggested that the maximum allowable CO_2 column height, which can be accommodated before the capillary barrier of the caprock is breached, can be found from $H_{max} = P_{cT} / (\rho_w - \rho_g)\, g$. Implicitly, an assumption is being made that there is hydrostatic conditions throughout both the caprock and the underlying reservoir. Some workers have suggested that Eq. (3) should be modified in order to take into account any overpressure, ΔP, in the water phase in the reservoir relative to the pressure in the water phase in the caprock (see Fig. 15). The maximum height of a gas or oil column that could be trapped by a seal would then be given by an equation of the form (Clayton and Hay, 1994)

$$H_{max} = (P_{cT} - \Delta P) / (\rho_w - \rho_g)\, g \qquad (6)$$

Note that under hydrostatic conditions $\Delta P = 0$. Consequently scenarios where $\Delta P \neq 0$ are sometimes referred to as hydrodynamic in this context (e.g. Underschultz, 2007; IEAGHG, 2011).

There has been significant technical debate as to whether the ΔP term should indeed be included in this way (Underschultz, 2007). Bjorkum et al. (1998) argue that in a water-wet system, there is a vertical pressure gradient between the aquifer at the free water level (FWL) (i.e., at the base of

the gas or oil column) and the top of the reservoir. If this is true, then there is only an infinitesimally small change in water pressure between the uppermost pore of the reservoir and the lowermost pore of the seal and thus excess pressure has no effect on H_{max}.

However, the relative permeability of water at the top of the reservoir is likely to be extremely small due to phase interference caused by the presence of gas and/or oil. Indeed it is often hypothesised that only the so-called irreducible water saturation should be present at the top of the reservoir. The term irreducible is used to imply that the water saturation cannot decrease below this point because of the absence of available permeability needed to displace the remaining water (i.e., it is trapped). Rodgers (1999) suggest that the permeability available to the water phase at the top of the reservoir should be sufficiently small such that excess pressure is incurred between the formation water pressure at the FWL and the formation water pressure at the top of the reservoir (Fig. 15). Accordingly, Rodgers (1999) reasserts that the ΔP term should be included and Eq. (6) is appropriate.

Teige et al. (2005) explored this problem further through laboratory experimentation and found that even at "irreducible water saturation" a sufficient amount of water is able to migrate through an oil (or gas) column into the caprock. This evidence is considered to refute the concerns of Rodgers (1999) and further supports Bjorkum et al.'s (1998) contention. Nevertheless, Underschultz (2007) provides some additional scenarios where the ΔP term can become more important, which the reader may want to study for further detail.

3.6 Expected CO_2 leakage through intact caprock

More recently, Hou et al. (2012) conducted an extensive numerical simulation exercise to explore the sensitivity of leakage, through an intact caprock, to various model parameters of concern. In total, 256 different CO_2 storage simulations were undertaken using the Pacific Northwest National Laboratory (PNL) reservoir simulator code, STOMP. From studying the statistics of the fraction of CO_2 leaked after 200 years, it was found that the parameters ranked in order of significance were (1) caprock thickness, (2) caprock permeability, (3) caprock porosity, (4) reservoir permeability and (5) reservoir porosity.

Fig. 16 summarises the sensitivity analysis to the top three parameters. The results suggest that providing the caprock thickness is greater than 50 m and the caprock permeability is less than 0.01 mD, it is unlikely that the mass of CO_2 leaked through the caprock, as a fraction of the total mass injected, is going to be greater than 10^{-5} (i.e., 0.001%).

4.0 Caprock integrity

4.1 Tensile and shear failure

Another major issue concerning risk of leakage through caprocks concerns whether or not the integrity of the caprock is maintained throughout the storage process. As CO_2 is injected into a reservoir formation, the pore-pressures within the reservoir will increase (Mathias et al., 2009; 2011). If unconstrained, increasing pore-pressures can lead to caprock failure. Three modes of failure are generally considered (Mathias et al., 2009):

1) Tensile failure of the intact rock
2) Shear failure of the intact rock

3) Re-shearing of existing fractures and faults

Tensile failure will occur when pore-pressures exceed the sum of the tensile strength and the minimum principal stress. Shear failure will occur when pore-pressure lead to the so-called Mohr circle intersecting with the so-called Coulomb failure line (see right hand side of Fig. 17).

In Fig. 17, σ_1 [Pa] and σ_3 [Pa] are the maximum and minimum principal stress, respectively and P_s [Pa] denotes the critical pore-pressure at which shear failure of critically aligned cohesionless faults occurs. Consideration of the Mohr circle diagram in Fig. 17 reveals that the shear-failure pressure, P_s, can be estimated from (see Jaeger et al., 2007, p. 92)

$$(\sigma_3 - P_s) / (\sigma_1 - P_s) = [(\mu^2 + 1)^{1/2} + \mu)]^{-2} \quad (7)$$

where $\mu = \tan \varphi$ and φ [deg] is the angle of friction of the rock of concern.

The critical pressure for cap rock failure to occur in tension, P_t [Pa], can be found from (see Jaeger et al., 2007, p. 99)

$$P_t = \sigma_3 + T_0 \quad (8)$$

where T_0 [Pa] is the tensile strength of the caprock.

By simple consideration of Coulomb's failure criterion, it is clear that re-shearing of pre-existing faults will occur before shear failure of the intact rock occurs, if one makes the conservative assumption that pre-existing faults may exist at all orientations. This is because (1) the intact rock will have a finite cohesion (the y-axis intercept in the Mohr circle) and (2) the angle of friction is likely to be larger for intact rock. On the basis of brittle failure plots, Sibson (2003) further argues that re-shearing should also precede the development of tensile fractures.

Tensile and shear failure of the intact rock can lead to the development of new fractures and hence potentially permeable pathways through the cap rock. These fractures will likely have significantly larger apertures than the pore-throats of original formation material. Therefore, such features will represent points where the capillary threshold pressure is greatly reduced.

Deformation induced fractures can also significantly enhance the permeability of anhydrite (De Paola et al., 2009; Hangx et al., 2010a) although Hangx et al. (2010b) showed through caprock flexure calculations that deformation induced permeability enhancement for the Zechstein is unlikely to occur in the context of most realistic CO_2 storage scenarios. Re-shearing of existing fractures and faults can also lead to significant permeability developments. This is discussed in further detail in the section on leakage through faults.

Fig. 17 (the left hand side) also shows possible pressure profiles with depth based on the initial conditions assumed by Rutqvist et al. (2008) (discussed in more detail later in this section). In this case, pore-pressure is assumed hydrostatic and an extensional regime is assumed whereby the minimum and maximum principal stresses are assumed to be in the horizontal and vertical directions, respectively. Horizontal stress, σ_h [Pa], is assumed to be related to vertical stress, σ_v [Pa], by $\sigma_h = 0.7\ \sigma_v$. Ignoring the tensile strength of the rock, tensile failure will occur when pore-pressures exceed the minimum principal stress. The corresponding critical shear-failure pressure,

can be calculated from Eq. (7). In Fig. 17, it can be seen, as argued by Sibson (2003), that the critical shear failure pressure is always less than the tensile failure criterion.

The assumption of hydrostatic pressure conditions in the SNSB tends to hold reasonably well due to the relative slow burial conditions attributed to that the region. Elsewhere, burial has been much more rapid and pore-pressures are significantly elevated. Fig. 18 shows a plot of pore-pressure and fracture pressure (essentially tensile failure pressure) for a range of reservoirs and caprock units in the Central North Sea. Fracture pressures were obtained using leakoff tests (see White et al., 2002 for more detail). Note how over pressure (the difference between pore pressure and hydrostatic pressure) continuously increases with depth. Also note the correlation between pore-pressure and fracture pressure.

4.2 Pore-pressure coupling

Rutqvist et al. (2008) argues that injection pressure and pore-pressure should be estimated in a simultaneously poroelastic coupled framework. Fig. 19 illustrates results from simulations using the TOUGH-FLAC framework. TOUGH2 is a multi-phase reservoir simulator. FLAC is a 3D rock mechanics code. TOUGH2 takes stress values from FLAC and calculates corresponding values of permeability and porosity. FLAC takes values of pore-pressure from TOUGH2 and establishes an updated stress field. It can be seen that the tensile and shear failure pressures increase with increasing pore-pressure (resulting from CO_2 injection).

Empirical evidence suggests that a simpler method for predicting pore-pressure coupling is to assume that the principal effective stress ratio remains constant, i.e. (Hillis, 2003)

$$(\sigma_3 - P) / (\sigma_1 - P) = C \qquad (9)$$

where P [MPa] is pore pressure and C [-] is a constant yet to be defined.

Assuming again an extensional environment (i.e., $\sigma_1 = \sigma_v$ and $\sigma_3 = \sigma_h$) and assuming σ_v remains constant, Eq. (9) can rearranged and differentiating with respect to P yeild

$$d\sigma_h / dP = (1 - C) \qquad (10)$$

It follows that minimum horizontal stress gradient should be a linear function of pore pressure gradient. An example for the Gannet/Guillemot Fields Area in the Noth Sea is shown in Fig. 20.

Goulty (2003) provides three conceptual models, which lead to different analytical expressions for C: (1) assuming normal compaction, $C = K_0$ where K_0 is known as the coefficient of earth pressure at rest; (2) assuming poroelastic behaviour and zero horizontal strain, $C = 1 - \alpha (1 - 2\nu) / (1 - \nu)$, where α [-] and ν [-] are the Biot coefficient and Poisson's ratio, respectively; (3) assuming critically stressed normal faults, $C = [(\mu^2 + 1)^{1/2} - \mu)]$.

For the hydrostatic and extensional initial condition assumed by Rutqvist et al. (2008), to obtain Fig. 19, it can be shown that $C = 0.4619$. Application of the final pore-pressure data (in Fig. 19) to Eq. (9) enables predictions of the final minimum principal stress and shear failure pressure shown in Fig. 21 as circular markers. The correspondence with the TOUGH2-FLAC simulation is remarkable (compare solid lines and circular markers). Of particular interest is that Eq. (9) ultimately suggests that the critical failure pressures continually increases with pore-pressure up

to the value of maximum principal stress, σ_1, which implies the only serious pressure constraint of concern is the lithostatic pressure, σ_v. Investigation is needed to better ascertain the validity of this approach further.

5.0 Summary and conclusions

In this section, the main focus has been on establishing a technical basis for understanding leakage of CO_2 through intact caprock systems. Recall that leakage through faults, fractures and wells is dealt with in subsequent sections of the report.

Relevant caprock systems for the UK North Sea consist of evaporites (halites and anhydrites) or shale formations of 100s to 1000s metres thickness (Gluyas and Hitchins, 2003). Caprock permeabilities are expected to be small with permeability for shales, anhydrites and halites ranging from 10^{-7} to 10^{-2} mD (Schlomer and Krooss, 1997), 10^{-6} to 10^{-4} mD (de Paola et al., 2010) and 10^{-9} to 10^{-6} mD (Evans and Holloway, 2009), respectively. A good reservoir seal is generally expected to have a permeability < 10^{-4} mD.

Low permeability implies low rates of leakage. However, more importantly for CO_2 sealing, low permeability implies that the rock matrix is comprised of very small pore-throat sizes (Leverett, 1940). The interfacial tension between CO_2 and brine within these small pore-throats can lead to zero leakage rates in many instances (Danial and Kaldi, 2008). The process of blockage due to interfacial tension is often referred to as capillary sealing.

Capillary sealing can be expected to occur providing the height of CO_2 column underneath a given caprock remains below a critical threshold. From the study of Naylor et al. (2011), it is expected that sustainable CO_2 column heights in Southern North Sea reservoirs are likely to be a factor of 0.7 to 1.3 of the size of gas column heights previously observed. A recent probabilistic analysis of Hou et al. (2012) suggests that providing caprock thickness is greater than 50 m and caprock permeability is less than 0.01 mD, the mass of CO_2 leaked through the caprock after 200 years is unlikely to be greater than 0.001% of the total injected mass.

The above studies assume that the caprock remains intact throughout. CO_2 is injected into a reservoir formation, pore-pressure is expected to increase. This can potentially lead to mechanical failure of the overlying caprock, leading to the development of new fractures and/or the reactivation of existing fractures and faults, all of which can lead to enhanced caprock permeability (Mathias et al., 2009).

5.1 Critical controls on leakage

Critical controls on leakage through caprocks include ability to maintain a capillary barrier, caprock permeability and whether or not the CO_2 injection leads to the development of tensile fractures or reactivation of existing faults or fractures.

5.2 Potential leakage rate

Providing the capillary seal is maintained, the CO_2 leakage rate through the caprock should be zero. If the capillary seal is broken, providing the caprock thickness is greater than 50 m and caprock permeability is less than 0.01 mD, the mass of CO_2 leaked through the caprock after 200 years is unlikely to be greater than 0.001% of the total injected mass. See section on leakage

through faults for discussion of possible leakage rates in the eventuality of tensile fracture development and fault reactivation.

5.3 Potential leakage duration

For all of the outcomes listed above, leakage will ultimately be driven by permeability, buoyancy drive and pressure gradient. For closed reservoirs, pressure is expected to decline with time. Caprock permeability and pressure gradient are both expected to reduce with reducing pressure. Consequently, CO_2 leakage rates can be expected to reduce with time. However, for open reservoirs, aquifer drive may lead to sustained reservoir pressures despite leakage. Consequently leakage may ultimately continue until the CO_2 reservoir is emptied of buoyant fluid.

5.4 Variation of risk through storage life cycle

The leakage scenarios described above are mostly reservoir pressure driven. The critical time for pressure is during injection. The risk of caprock failure dramatically decreases once CO_2 injection is stopped. Following CO_2 injection the probability of caprock failure will be mostly driven by externally induced seismic events or nearby reservoir engineering activity (e.g. oil and gas or new CO_2 storage projects).

6.0 References

Beauheim, R. L., Roberts, R. M. (2002) Hydrology and hydraulic properties of a bedded evaporate formation. Journal of Hydrology. 259:66-88.

Bennion, D. B., Bachu, S. (2007) Permeability and relative permeability measurements at reservoir conditions for CO_2-Water systems in ultralow-permeability confining caprocks. SPE Europec/EAGE Annual Conference and Exhibition held in London, UK. SPE 106995.

Bjorkum P. A., Walderhaug O., Nadeau P. H. (1998) Physical constraints on hydrocarbon leakage and trapping revisited. Petroleum Geoscience. 43:237–9.

Chadwick, A., Williams, G., et al. (2010) Quantitative analysis of time-lapse seismic monitoring data at the Sleipner CO_2 storage operation. The Leading Edge. February 2010:170-177.

Chalbaud, C., Robin, M., Lombard, J. M., Martin, F., Egermann, P., Bertin, H. (2009) interfacial tension measurements and wettability evaluation for geological CO_2 storage. Advances in Water Resources. 32:98-109.

Chiquet, P., Broseta, D., Thibeau, S. (2007) Wettability alteration of caprock minerals by carbon dioxide. Geofluids 7: 112-122.

Clayton, C. J., Hay, S. J. (1994) Gas migration mechanisms from accumulation to surface. Bulletin of the Geological Society of Denmark. 41:12–23.

Danial, R. F., Kaldi, J. G. (2008) Evaluating seal capacity of caprocks and intraformational barriers for the geosequestration of CO_2. PESA Eastern Australian Basins Symposium III. Sydney, 14–17 September, 2008. 475-484.

De Paola, N. Faulkner, D. R., Collettini, C. (2009) Brittle versus ductile deformation as the main control on the transport properties of low porosity anhydrite rocks. Journal of Geophysical Research. 114:B06211.

Duguid, C., Underhill, J. R. (2010) Geological controls on Upper Permian Plattendolomit Formation reservoir prospectivity, Wissey Field, UK Southern North Sea. Petroleum Geoscience. 16:331-348.

Evans D. J., Holloway S. (2009) A review of onshore UK salt deposits and their potential for underground gas storage. Evans, D. J. & Chadwick, R. A. (eds) Underground Gas Storage: Worldwide Experiences and Future Development in the UK and Europe. The Geological Society, London, Special Publications. 313:39–80.

Gaarenstroom, L., Tromp, R. A. J., de Jong, M. C., Brandenburg, A. M. (1993) Overpressures in the Central North Sea: implications for trap integrity and drilling safety. Petroleum Geology of Northwest Europe: Proceedings of the 4th Conference (edited by J. R. Parker). Petroleum Geology '86 Ltd. Published by The Geological Society, London, pp. 1305-1313.

Gluyas, J.G. and Hichens, H. (2003) North Sea Oil and Gas Fields - Millennium Review, Geological Society of London Memoir **20,** 1006pp

Goulty, N. R. (2003) Reservoir stress path during depletion of Norwegian chalk oilfields. Petroleum Geoscience. 9:233–241.

Hangx, S. J. T., Spiers, C. J., Peach, C. J. (2010a) The effect of deformation on permeability development in anhydrite and implications for caprock integrity during geological storage of CO_2. Geofluids. 10:369-387.

Hangx, S. J. T., Spiers, C. J., Peach, C. J. (2010b) Mechanical behaviour of anhydrite caprock and implications for CO_2 sealing capacity. Journal of Geophysical Research. 115:B07402.

Haszeldine, S., Lu, J., Wilkinson, M. And Macleod, G. (2006) Long-timescale interaction of CO_2 storage with reservoir and seal: Miller and Brae natural analogue fields North Sea, Greenhouse Gas Control Technology 8, Trondheim, 19-22 June 2006, Elsevier

Hillis, R. R. (2003) Pore pressure/stress coupling and its implications for rock failure. Van Rensbergen, P., Hillis, R. R., Maltman, A. J., Morley, C. K. (eds) Subsurface Sediment Mobilization. Geological Society, London, Special Publications, 216:359-368.

Horsrud, P., Sonstebo, E. F., Boe, R. (1998) Mechanical and petrophsyical properties of North Sea shales. Int. J. Rock Mech. Min. Sci. 34:1009-1020.

Hou, Z., Rockhold, M. L., Murray, C. J. (2012) Evaluating the impact of caprock and reservoir properties on potential risk of CO_2 leakage after injection. Environ. Earth Sci. In Press doi:10.1007/s12665-011-1465-2.

Huet, C. C., Rushing, J. A. et al. (2005) A modified Purcell/Burdine model for estimating absolut permeability from mercury-injection capillary pressure data. International Petroleum technology Conference held in Doha, Qatar, 21-23 November 2005. IPTC 10994.

IEAGHG (2011) Caprock Systems for CO_2 Geological Storage. IEAGHG, Cheltenham, UK.

Jaeger, J. C., Cook, N. G. W., Zimmerman, R. W. (2007) Fundamentals of Rock Mechanics. Wiley–Blackwell, Oxford.

Leverett, M. C. (1940) Capillary behaviour in porous solids. Trans AIME 142:341-358.

MacMinn, C. W., M. L. Szulczewski and R. Juanes (2011) CO_2 migration in saline aquifers. Part 2: Capillary and solubility trapping. Journal of Fluid Mechanics. 688:321-351.

Mathias, S. A., Hardisty, P. E., Trudell, M. R., Zimmerman, R. W. (2009) Screening and selection of sites for CO_2 sequestration based on pressure buildup. International Journal of Greenhouse Gas Control 3(5): 577-585.

Mathias, S. A., Gluyas, J. G., Gonzalez, G., Hosseini, S. (2011) Role of partial miscibility on pressure buildup due to constant rate injection of CO_2 into closed and open brine aquifers. Water Resources Research 47: W12525.

Naylor, M., Wilkinson, M., Haszeldine, R. S. (2011) Calculation of CO_2 column heights in depleted gas fields from known pre-production gas column heights. Marine and Petroleum Geology 28:1083-1093.

Pape, H., Clauser, C., Iffland, J. (2000) Variation of permeability with porosity in sandstone diagenesis interpreted with a fractal pore space model. Pure Appl. Geophys. 157:603-619.

Ringrose, P., Eiken, E., et al. (2011) Sleipner and Snøhvit Projects. CSLF Interactive Workshop, Saudi Arabia. 01-02 March 2011.

Rodgers S. (1999) Discussion: 'Physical constraints on hydrocarbon leakage and trapping revisited' by Bjørkum et al. – further aspects. Petroleum Geoscience. 5:421–423.

Rutqvist, J., Birkholzer, J. T., Tsang, C.-F. (2008) Coupled reservoir–geomechanical analysis of the potential for tensile and shear failure associated with CO_2 injection in multilayered reservoir–caprock systems. International Journal of Rock Mechanics & Mining Sciences. 45:132–143

Schlomer, S., Krooss, B. M. (1997) Experimental characterisation of the hydrocarbon sealing efficiency of cap rocks. Marine and Petroleum Geology. 14:565-580.

Sibson, R. (2003). Brittle-failure controls on maximum sustainable overpressure in different tectonic regimes. AAPG Bull. 87 (6), 901–908.

Swanson, B. F. (1981) A simple correlation between permeabilities and mercury capillary pressures. Journal of Petroleum Technology. (Dec 1981) 2498-2504.

Taylor, J. C. M. (1998) Upper Permian – Zechstein. Glennie, K. W. eds. Petroleum Geology of the North Sea – Basic Concepts and Recent Advances. 174-211.

Teige, G. M. G., C. Hermanrud, W. L. H. Thomas, O. B.Wilson And H. M. Nordgard Bolas (2005) Capillary Resistance And Trapping Of Hydrocarbons: A Laboratory Experiment. Petroleum Geoscience. 11:125-129.

Underschultz, J. (2007) Hydrodynamics and membrane seal capacity. Geofluids. 7:148-158

White, A.J., Traugott, M. O and Swarbrick, R.E. (2002) The use of leak-off tests as means of predicting minimum in-situ stress. Petroleum Geoscience, 8:189-193.

Wollenweber, J., Alles, S., Busch, A., Krooss, B. M., Stanjek, H., Littke, R. (2010) Experimental investigation of the CO_2 sealing efficiency of caprocks. International Journal of Greenhouse Gas Control. 4:231-241.

Yielding, G., Lykakis, N., Underhill, J. R. (2011) The role of stratigraphic juxtaposition for seal integrity in proven CO_2 fault-bound traps of the Southern North Sea. Petroleum Geoscience. 17:193-203.

7.0 Tables and figures

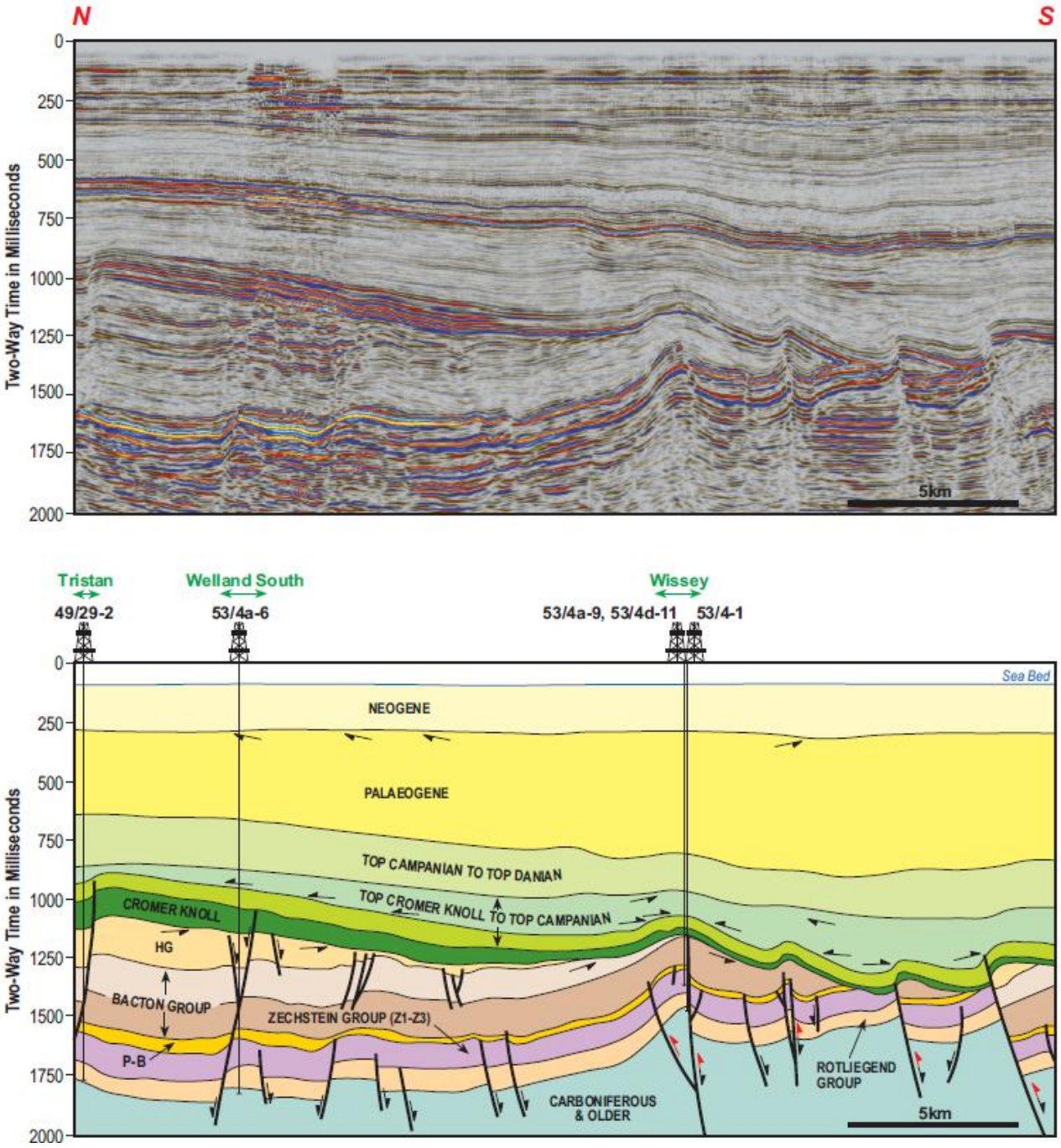

Fig 1a: Typical seismic section and associated interpretation illustrating some key geological features of the Southern North Sea (Duguid and Underhill, 2010).

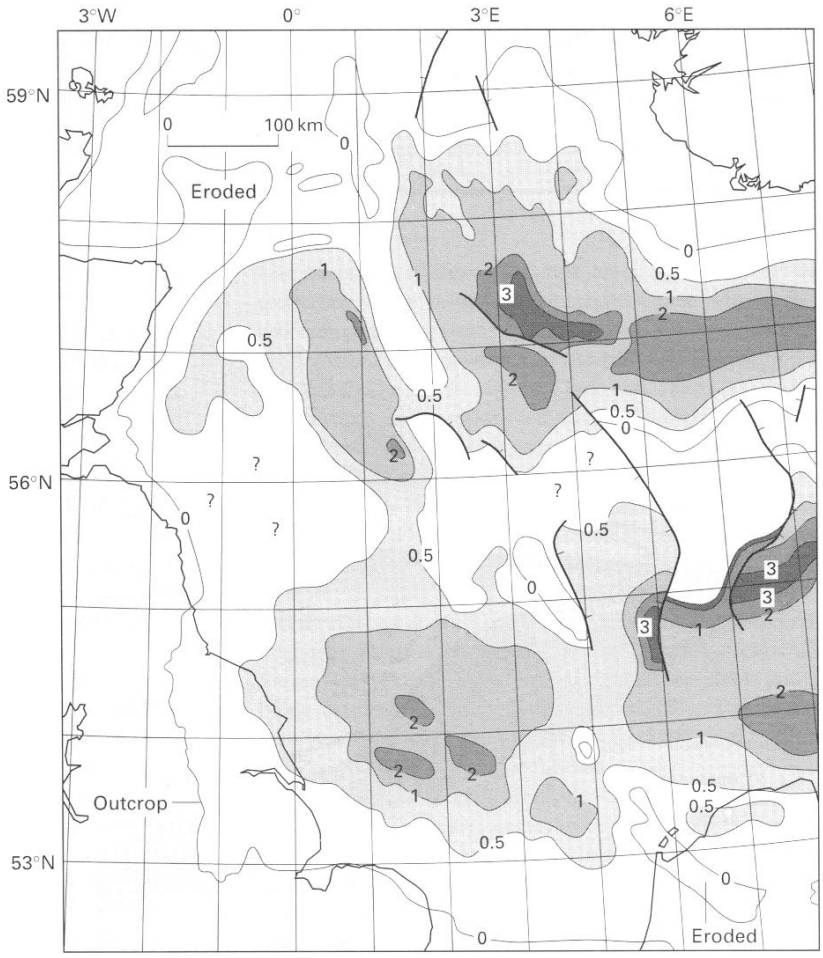

Fig 1b: Average thickness of the Zechstein in km (after Taylor, 1998).

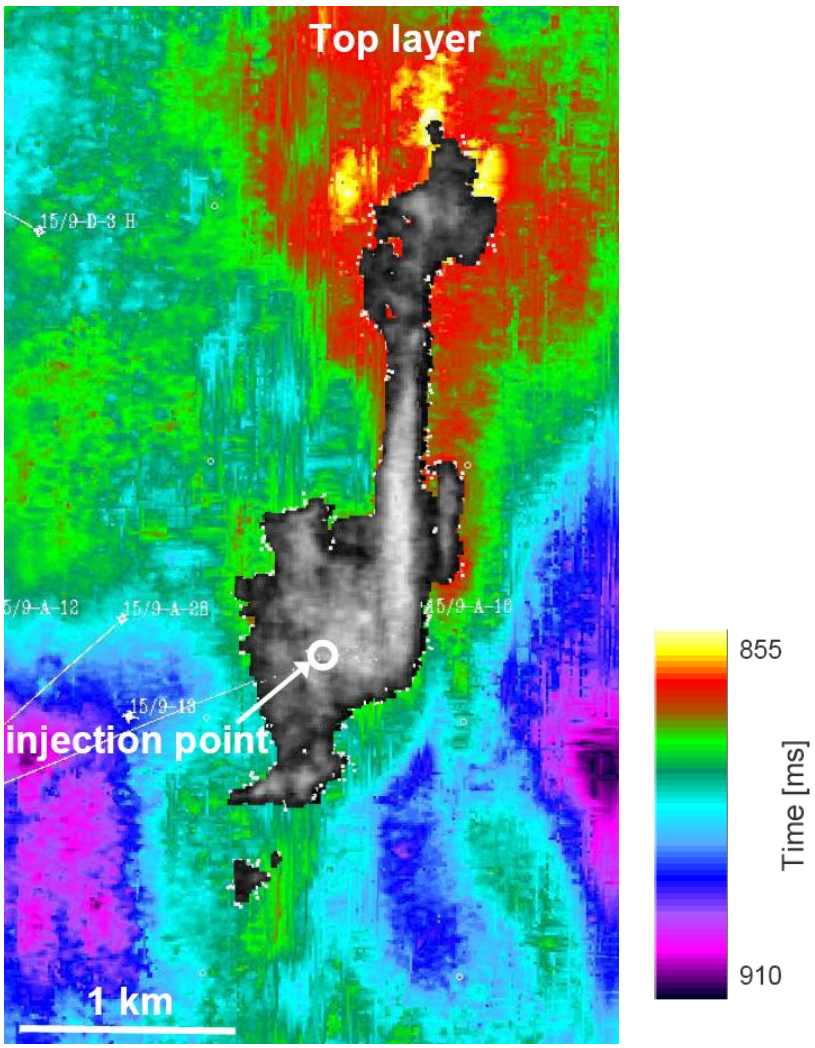

Fig. 2: Results from time-lapse seismic of the CO_2 plume at Sleipner in 2008 (Ringrose et al., 2011). The color-scale is for the underside topography of the caprock. CO_2 is seen to follow the topography of accumulating in the highest points.

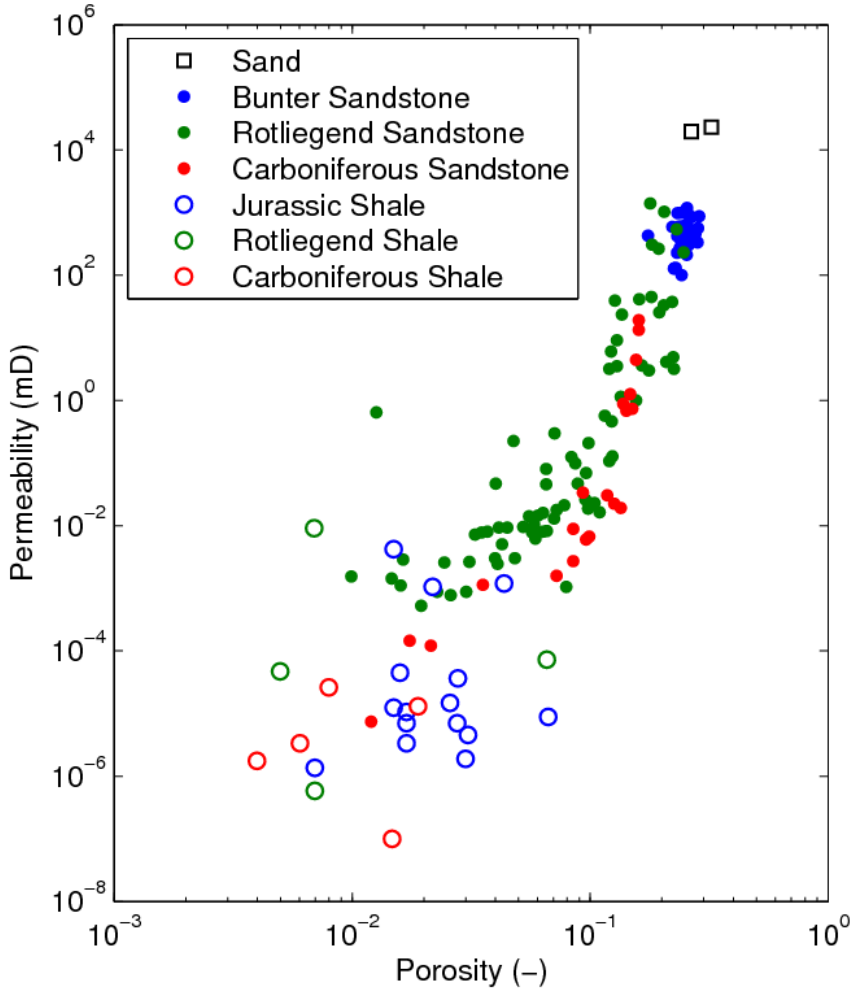

Fig. 3a: Permeability and porosity data for some Southern North Sea rocks (after Pape et al., 2000).

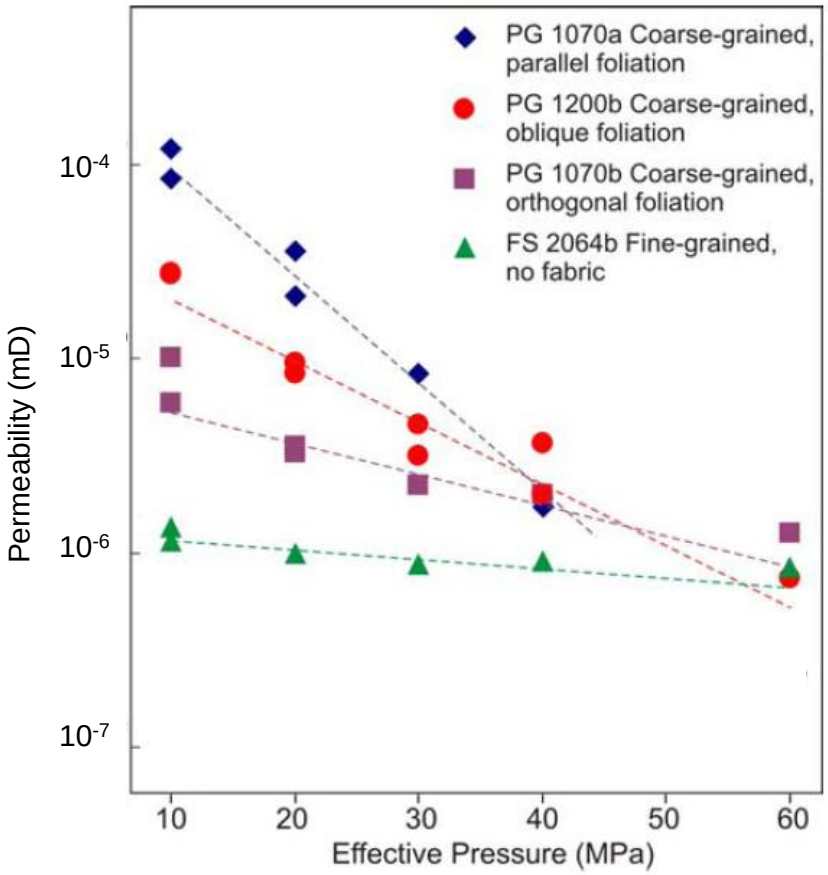

Fig 3b: Static permeability values for anhydrite samples from the Umbria-Marche Apennines, measured under hydrostatic stress conditions, for different values of the effective pressure, for samples with different grain size and fabric orientation (de Paola et al., 2009).

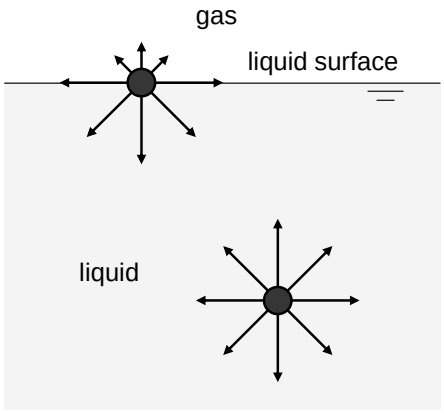

Fig. 4: Liquid molecules experience greater attraction to molecules of the same fluid than molecules of other fluids. Consequently an interface develops and liquids behave as if covered by an elastic membrane in a constant state of tension.

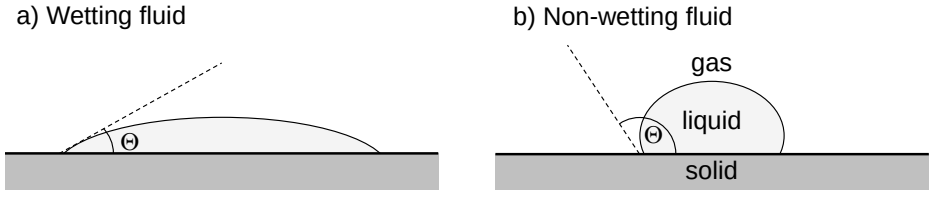

Fig. 5: Illustration of how a contact angle describes wettability.

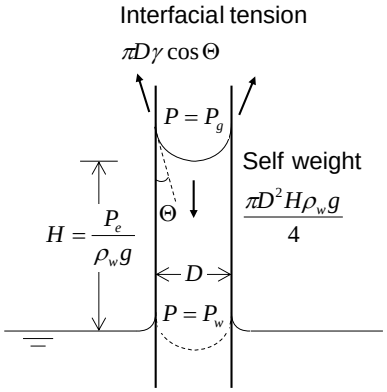

Fig. 6: Schematic diagram of a capillary tube.

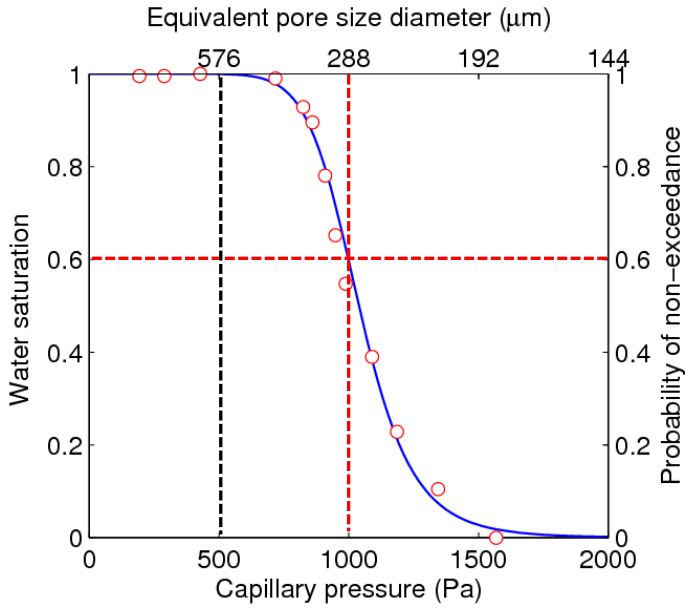

Fig. 7: A capillary pressure curve and its correspondence to a pore-size distribution.

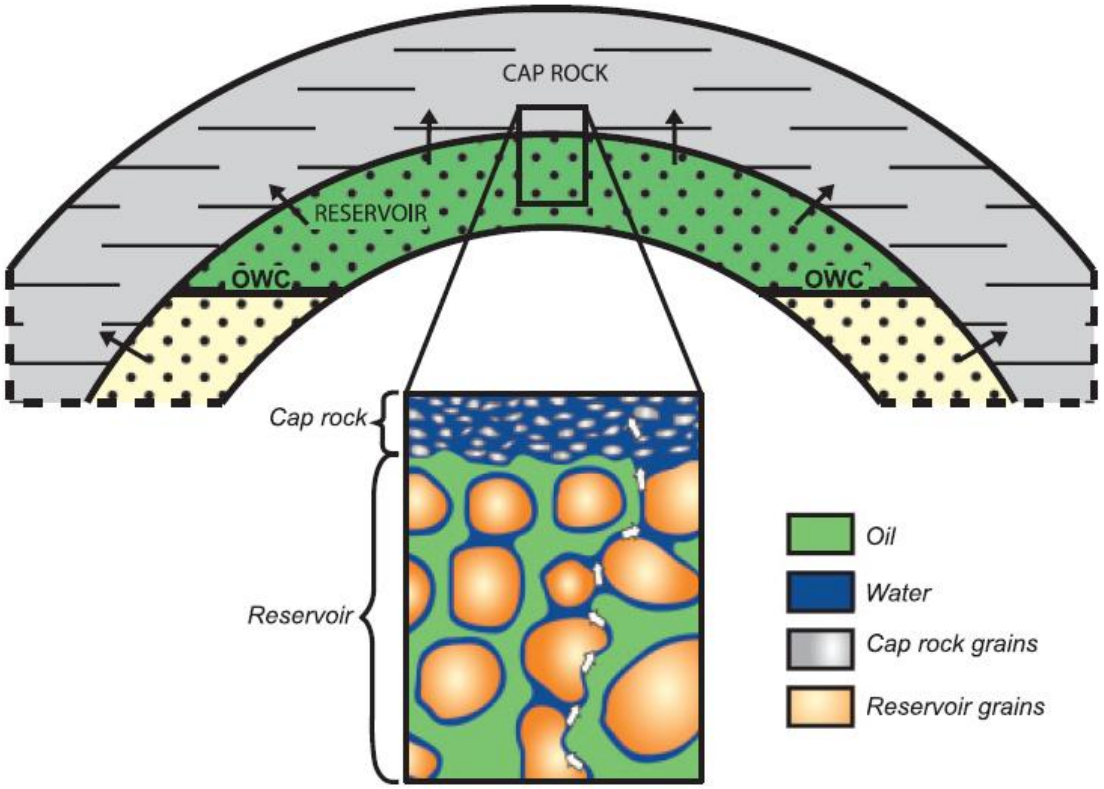

Fig. 8: The concept of water flow through an oil-saturated reservoir (after Teige et al., 2005).

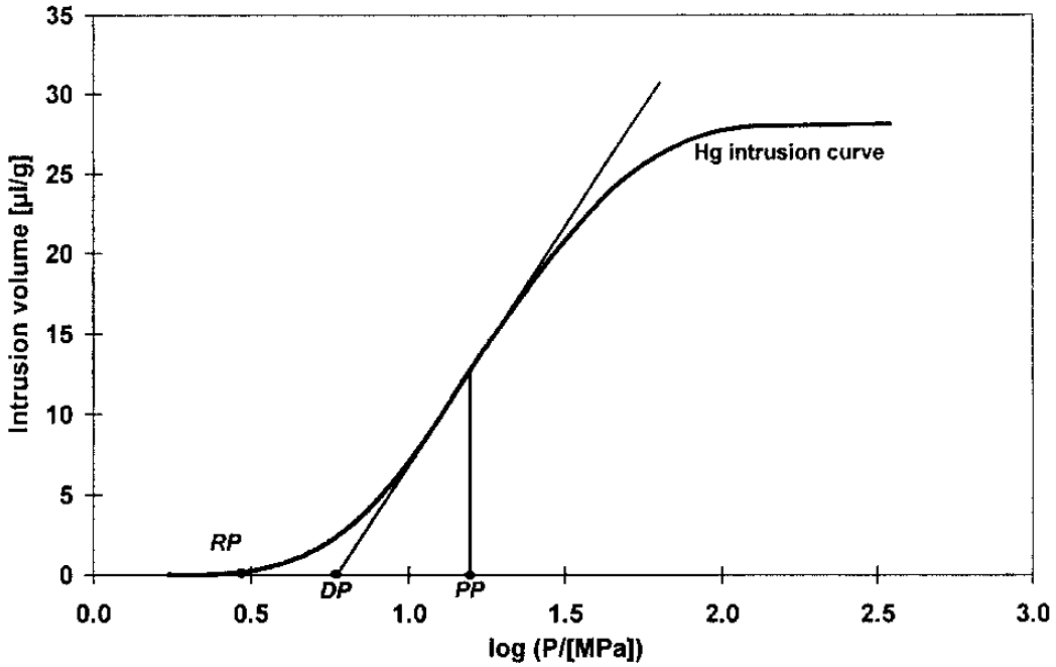

Fig. 9: Estimation of capillary threshold pressure by mercury intrusion (Schlomer and Krooss, 1997).

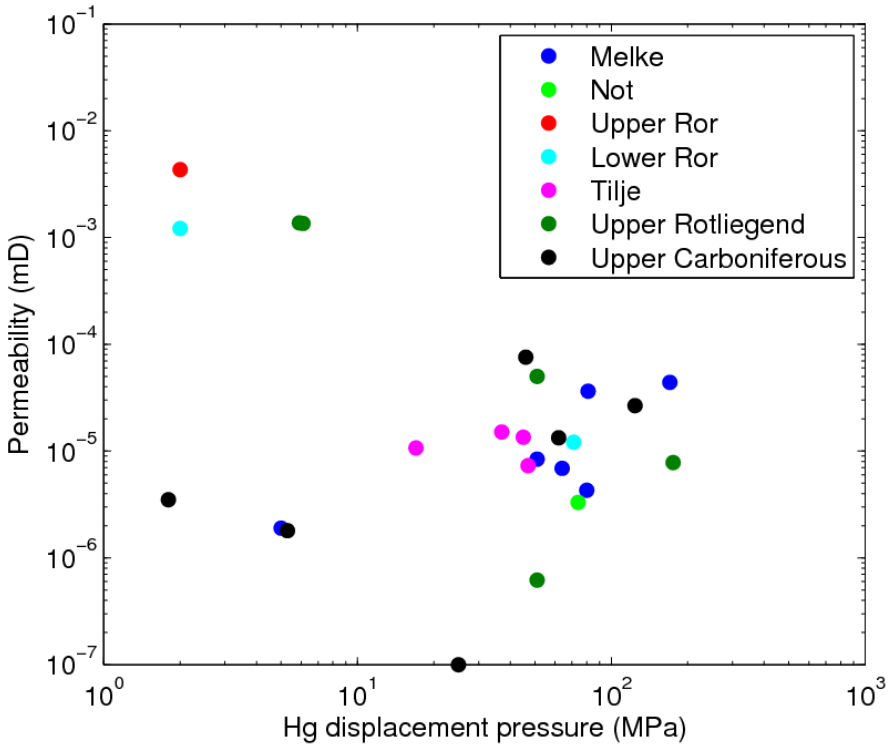

Fig. 10: A plot of mercury displacement pressure against permeability for a number of North Sea shales (after Schlomer and Krooss, 1997).

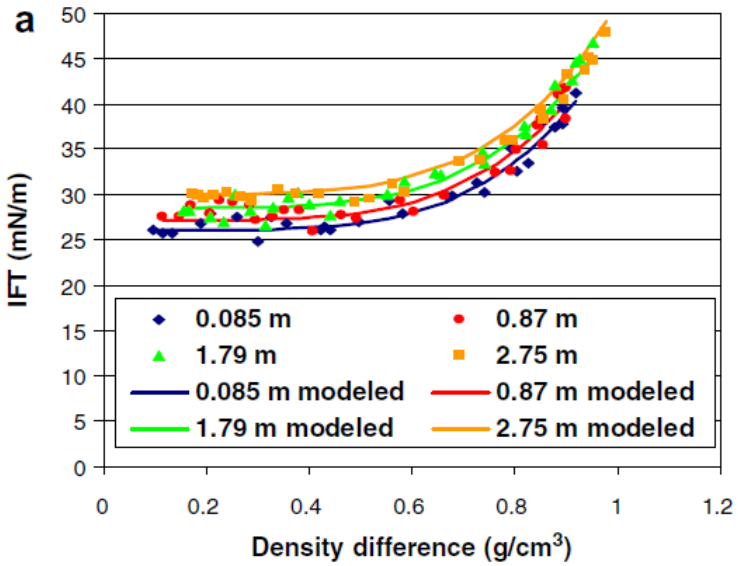

Fig. 11: Interfacial tension (IFT) for CO_2 and brine mixtures (after Chalbaud et al., 2009).

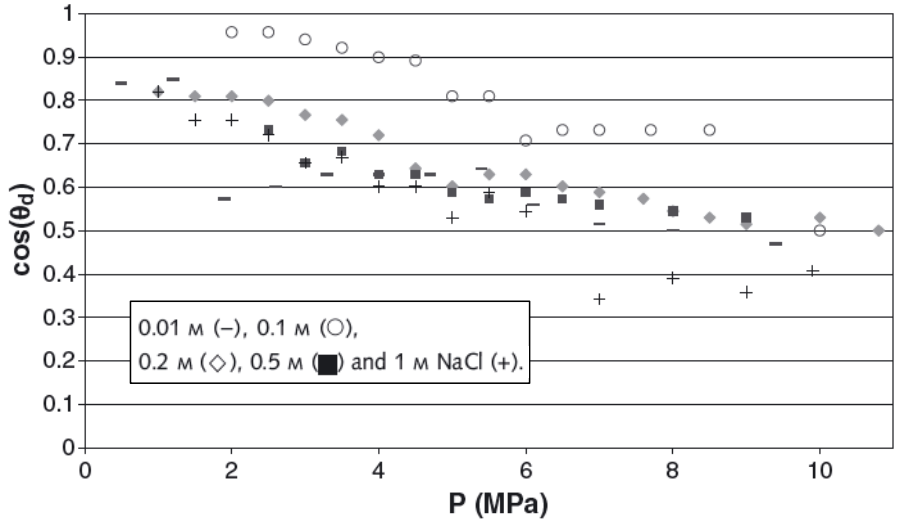

Fig. 12: Drainage contact angles for CO_2 and brine mixtures on mica as a function of pressure (after Chiquet et al., 2007).

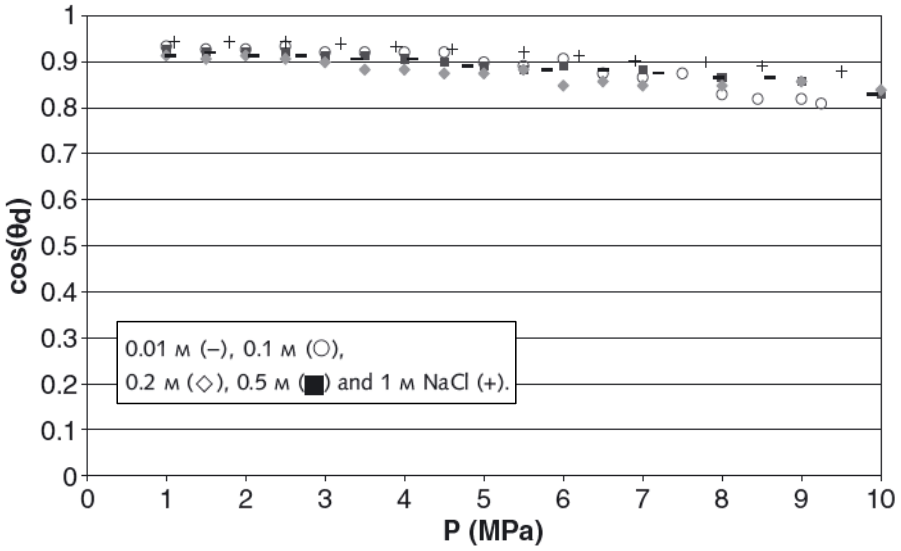

Fig. 13: Drainage contact angles for CO_2 and brine mixtures on quartz as a function of pressure (after Chiquet et al., 2007).

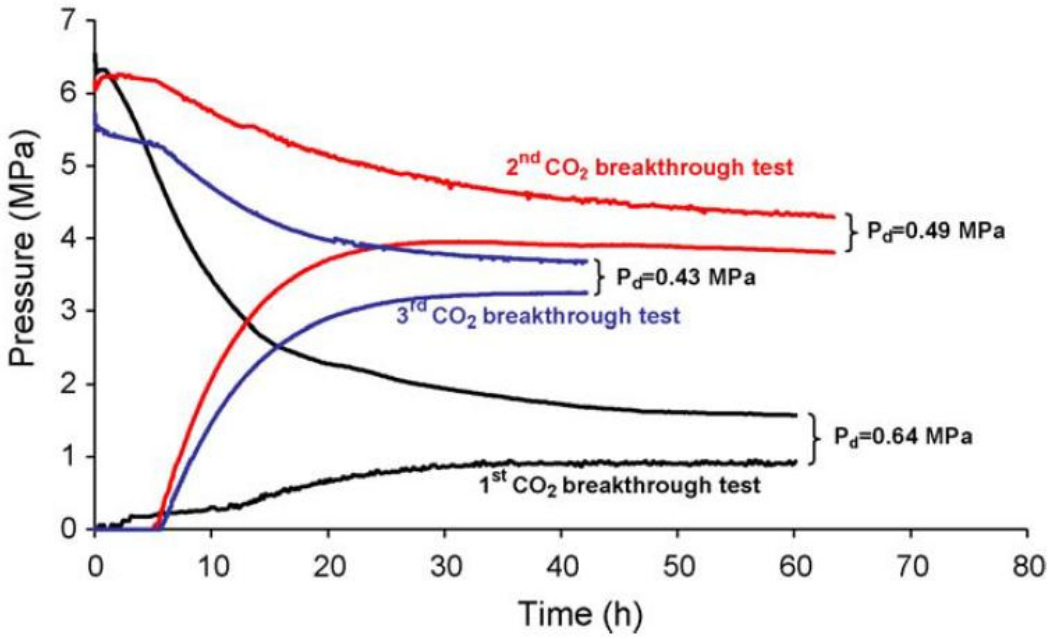

Fig. 14: Repetitive CO_2 breakthrough test of a Cretaceous marlstone caprock from the Munsterland Basin (Wollenweber et al., 2010).

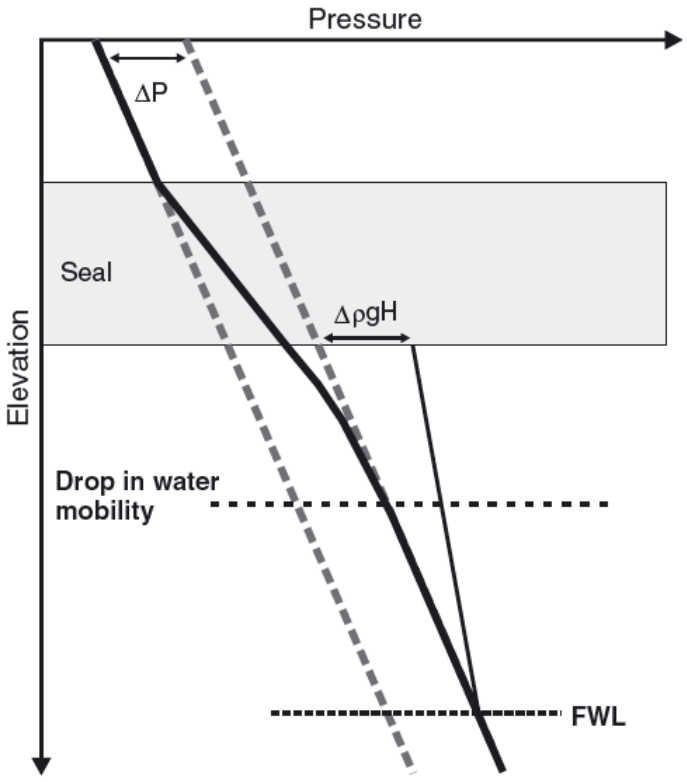

Fig. 15: Excess pressure within a hydrocarbon column (after Rodgers 1999).

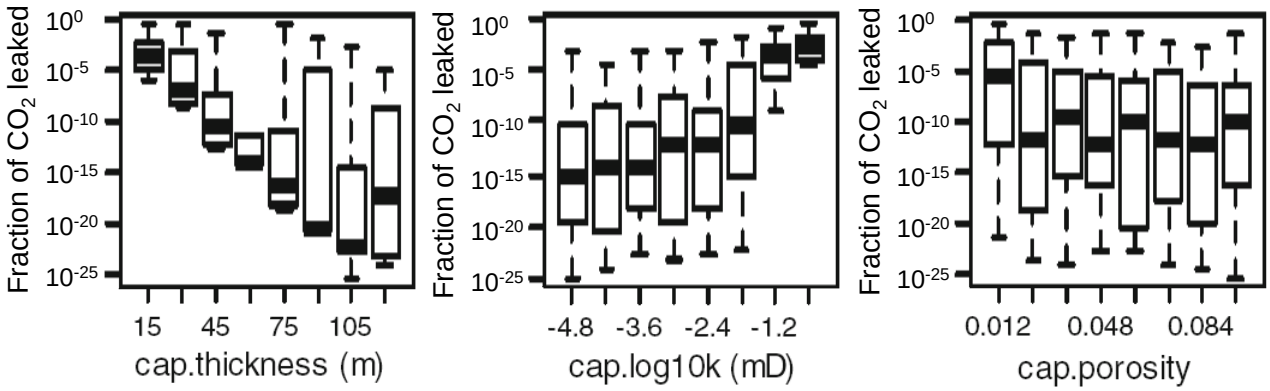

Fig. 16: Box plots for fraction of CO_2 leaked after 200 years showing results from the multivariate sensitivity analysis of Hou et al. (2012) (see text for further details).

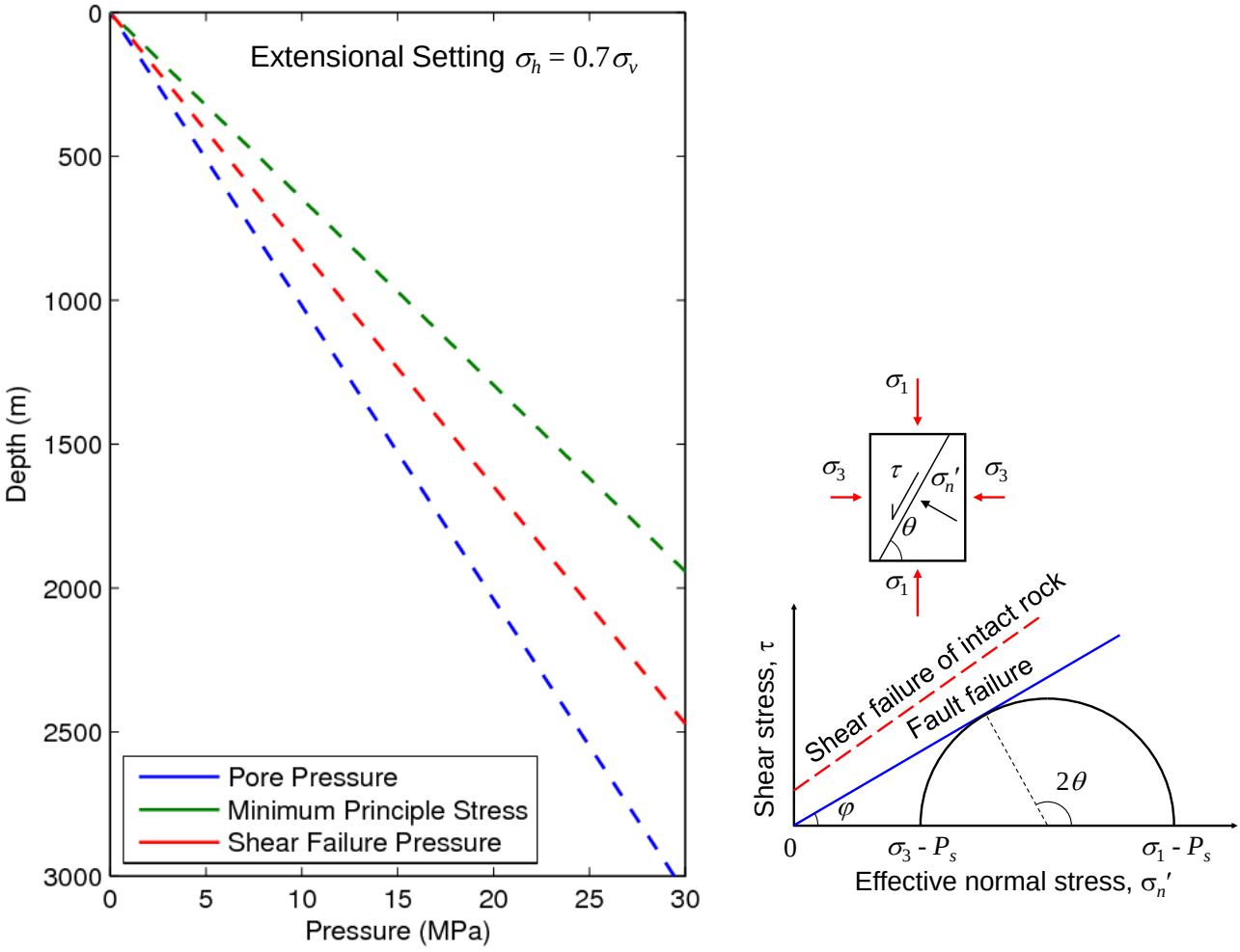

Fig. 17: Comparison of minimum principle stress against a shear failure pressure associated with re-shearing of critically aligned existing faults. The critical pore-pressure for shear failure of critically aligned faults can be obtained by considering the trigonometry of the Mohr circle shown on the right.

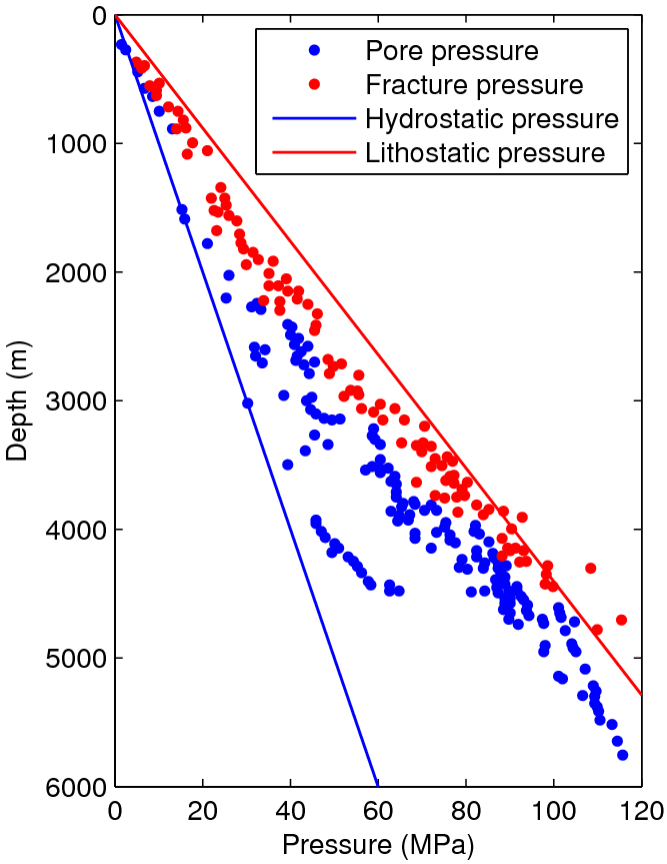

Fig. 18: Pore pressures and fracture pressures for a number of reservoirs from the Central North Sea (after Gaarenstroom et al., 1993).

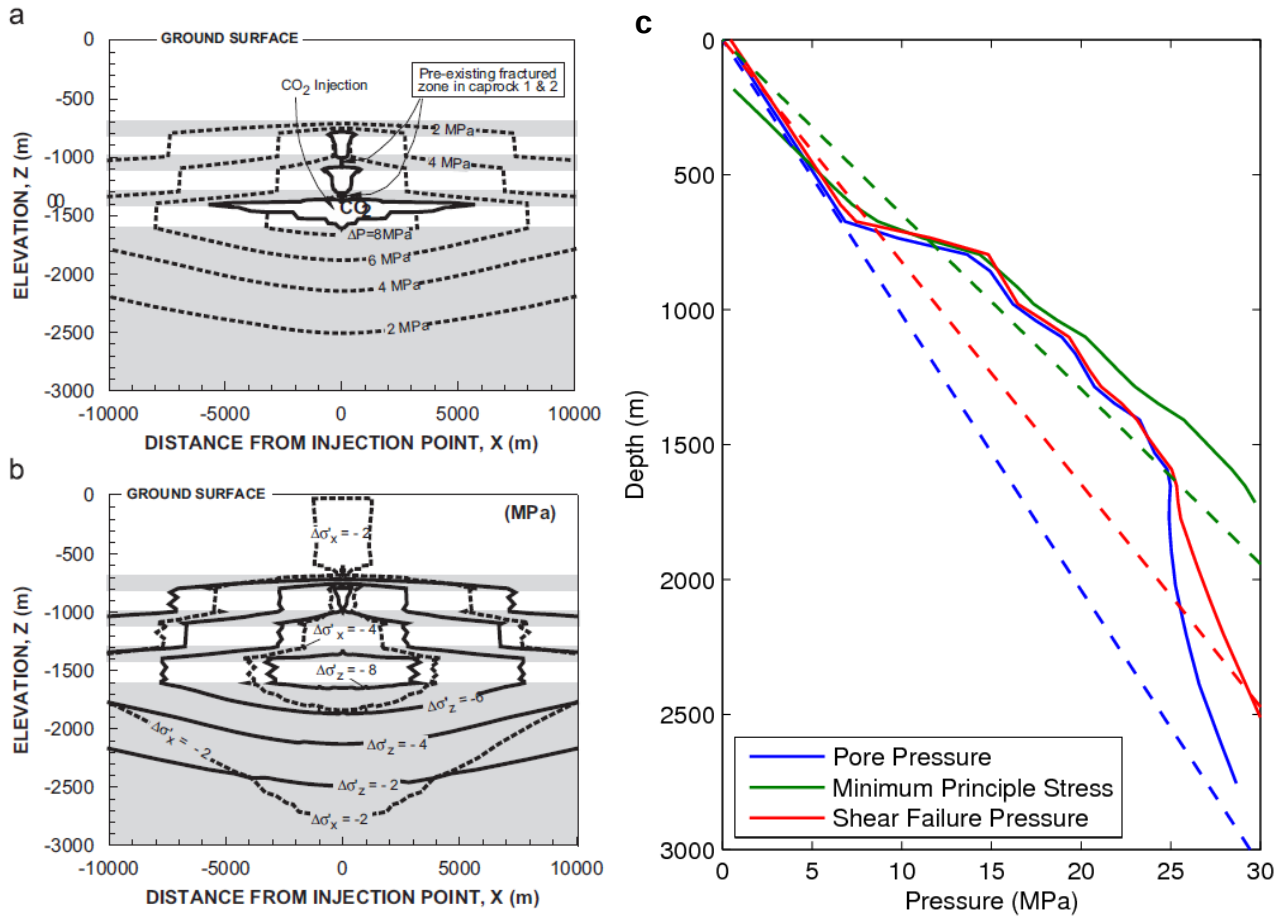

Fig. 19: Evolution of failure criterion with increasing pore-pressure (after Rutqvist et al., 2008). On the left hand side, a) shows contour plots of pore pressure and b) shows contour plots of changes in vertical and horizontal effective stress. The right hand side shows pore pressure, minimum principle stress and shear failure pressure associated with re-shearing of critically aligned existing faults, with the dashed and solid lines representing the initial and final conditions, respectively.

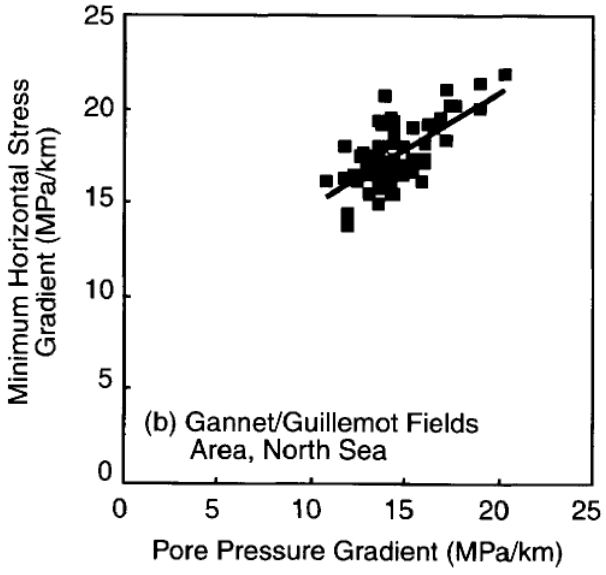

Fig. 20: Pore pressure gradient versus minimum horizontal stress gradient plot for Gannet and Guillemot Fields of the North Sea showing increasing minimum horizontal stress with increasing pore pressure Hillis (2003).

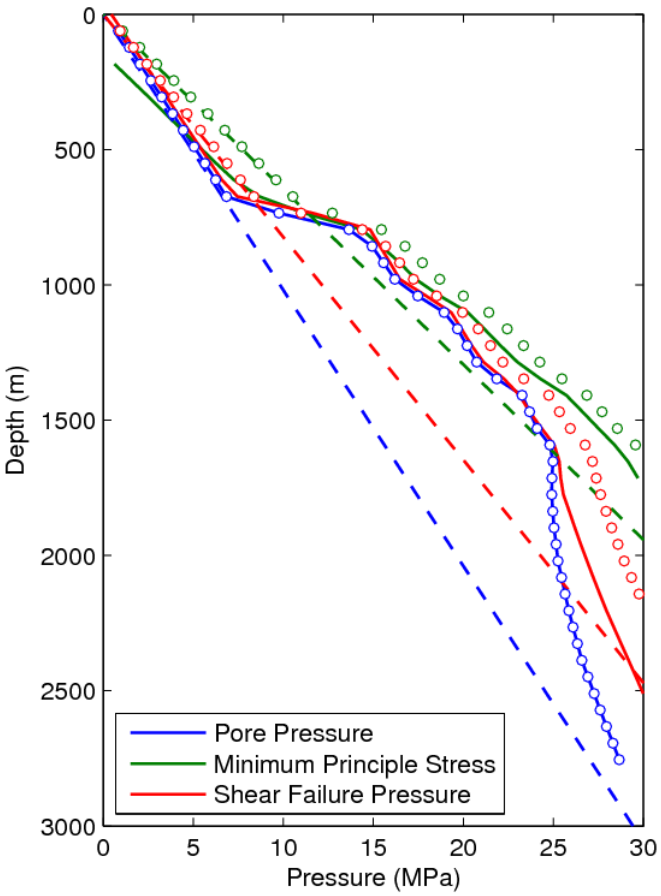

Fig. 21: A comparison of failure criterion predication assuming constant effective stress (the circular markers) with those from the hydromechanical modelling of Rutqvist et al. (2008) (the solid lines).